Pergamon

Applied Thermal Engineering Vol. 16, Nos 8/9, pp. 741–752, 1996

1359-4311(95)00063-1
1359-4311/96 $15.00 + 0.00

FLOW DISTORTIONS AT THE FAN INLET OF FORCED-DRAUGHT AIR-COOLED HEAT EXCHANGERS

K. Duvenhage, J. A. Vermeulen, C. J. Meyer and D. G. Kröger*
Department of Mechanical Engineering, University of Stellenbosch, Stellenbosch, South Africa

(*Received* 7 *October* 1995)

Abstract—The effect of inlet flow distortions on fan performance in forced-draught air-cooled heat exchangers (ACHEs) is investigated numerically and experimentally. By varying the distance between the ACHE fan platform and the ground level, significant changes in air volume flow rate are observed. Three different fan inlet shrouds are considered and recommendations towards designing and evaluating the performance of an ACHE are made. The effect of different lengths of a cylindrical fan inlet shroud, as well as the effect of cylindrical sections as part of a conical and a bell-mouth inlet shroud, is also investigated. The results show that a critical length for both the cylindrical inlet shroud and the cylindrical sections of the conical and bell-mouth inlet shrouds can be obtained for optimal fan performance.

Keywords—Air-cooled heat exchanger, forced-draught, axial fan, flow distortions, inlet shroud.

NOMENCLATURE

A	area
ACHE	air-cooled heat exchanger
C	chord
C_1, C_2, C_μ	constants in turbulence equations
C_D	drag coefficient
C_L	lift coefficient
c_p	specific heat
d	diameter
Eu	Euler number
F	force
g	gravitational acceleration
G	production term
h	heat transfer coefficient
H	height
k	turbulent kinetic energy
K	pressure drop coefficient
m	mass flow rate
n	number
p	pressure
Pr	Prandtl number
Q	torque
r	radius
R	gas constant
S	source term
t	thickness
T	temperature or thrust
U	overall heat transfer coefficient
v	velocity
V	Volume flow rate
$\vec{v}$	velocity vector
x,y,z	coordinates

Greek letters

ε	dissipation rate of turbulent kinetic energy
β	relative angle
Γ	diffusion coefficient
θ	relative angle
μ	dynamic viscosity
ρ	density

*Author to whom correspondence should be addressed.

σ	Prandtl number for k and ε
ϕ	general variable
Ψ	rotor solidity

Subscripts

a	air
aa	ambient air
B	buoyancy
bell	bell-mouth
c	contraction
cs	cylindrical section
e	effective
f	fluid
F/b	fans per bay
Fb	fan blade
fr	frontal
Fr	fan rotor
he	heat exchanger
i	inlet
max	maximum
o	outlet
r	relative
ref	reference
s	shroud
t	turbulent
tb	tube bundle
x,y,z	coordinates
θ	angle
ϕ	related to specific variable

INTRODUCTION

Forced-draught air-cooled heat exchangers (ACHEs) are extensively used for cooling duties in petroleum and chemical industries. When designing or evaluating the performance of an ACHE, one of the most important aspects is determining the system flow resistance characteristic. This characteristic curve, in conjunction with the fan performance curve, is used to determine the exact operating point of the ACHE. It is therefore important that the system flow losses are correctly predicted for a good design.

Most of the major losses in an ACHE system are well documented [1]. One of the losses in the system that is poorly documented is the effect due to inlet flow distortions on the fan performance in forced-draught ACHEs. Flow distortions or disturbances at the inlet to the fans can adversely affect the fan performance and will have a negative influence on the thermal performance of the ACHE.

Turner [2] found during tests on a full-scale ACHE that flow separation at the fan inlet cone will cause maldistribution of air at the fan inlet and a corresponding reduction in fan performance. Although this flow separation at the inlet cone was brought about by cross winds, the same situation will occur if the approach velocity at the edges of the ACHE is too high. Monroe [3] attempted to address this problem by stating that designers should insure that the air velocity at the entrance to the fan is no more than approximately one-half of the velocity through the fan throat. A certain amount of experimental work has since been carried out on forced-draught ACHEs for different fan inlet shrouds [4–7]. This paper is an attempt to collate these experimental data and to introduce new numerically and experimentally derived data.

Forced-draught ACHEs in the petroleum and chemical industries are usually mounted in long banks. A bay usually consists of two side-by-side tube bundles with two axial flow fans, with their axes in the vertical position, fitted to each bay. These bays are then placed side-by-side to form an ACHE bank. Sets of bays 16 or more long are very common. Each fan is surrounded on three sides by other fan intakes and in windless conditions essentially all the air to a single fan will be drawn in from one side of the ACHE. Figure 1 shows a part of a long (essentially two-dimensional) ACHE bank, showing the symmetry planes across which air flow will not occur in windless conditions. The flow patterns through the ACHE bank can therefore be predicted by considering only one axial fan blocked off on three sides.

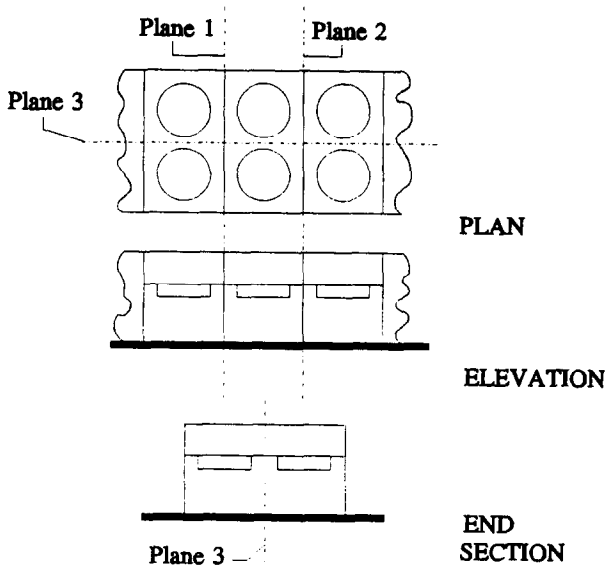

Fig. 1. Diagram of a long ACHE bank showing the planes over which flow will not occur.

NUMERICAL MODEL

The general-purpose code, PHOENICS, for numerical simulations of fluid flow, heat transfer and chemical-reaction processes is used to simulate a fan unit which is a part of a long, essentially two-dimensional ACHE bank, as shown in Fig. 1. The ACHE has a frontal tube bundle area of $7.07 \times 10.2 = 72.12$ m^2 per bay, a tube bundle height of 0.72 m, a plenum height of 1.7 m. Each bay contains two six-blade, 4.31-m diameter axial flow fans with cylindrical inlet shrouds. The main dimensions of a bay of the ACHE bank are given in Fig. 2.

The axial fan is modelled with the aid of the blade element theory as described by ref. [8]. This theory which is commonly employed for aircraft and ship propeller calculations was adapted by Thiart and Von Backström [8] and successfully employed in simulating the flow field near an axial fan operating under distorted inflow conditions.

The influence of the fan blades are modelled as body forces exerted on the air. Each blade element between two radii r and $(r + \delta r)$ experiences a lift force, δL, and a drag force, δD. It is assumed that there are no radial forces. These two forces are, respectively, normal and parallel to a relative velocity vector, $\vec{v}_r$. This relative velocity vector is composed of the axial velocity component and the azimuthal velocity component of the air relative to the blade element. By decomposing the lift

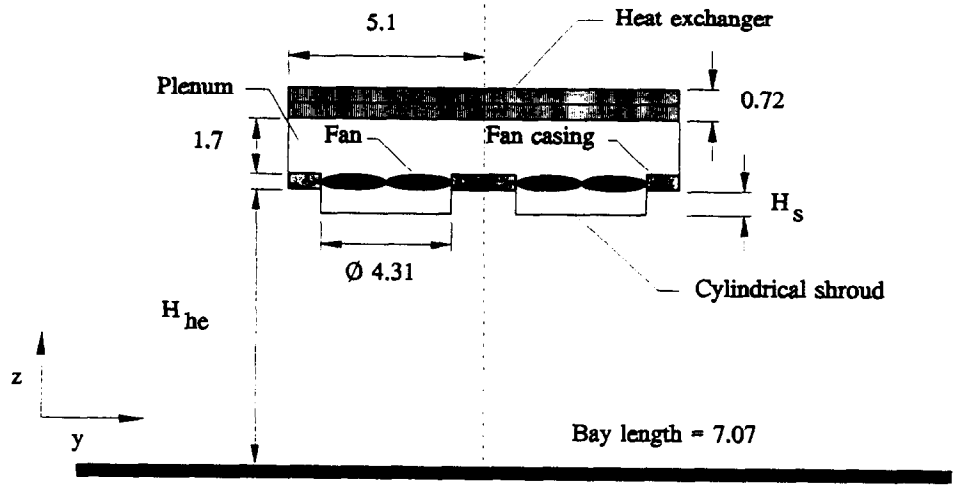

Fig. 2. A single bay of a long ACHE bank (dimensions in metres).

and drag forces into axial and azimuthal components, the thrust and torque exerted by the blade element on the air are obtained. Body forces appear in the Navier–Stokes equations as forces per unit volume. The thrust and torque per unit volume exerted by a blade element on the air are given by, respectively,

$$\frac{\partial T}{\partial V} = \frac{1}{2}\rho_a \bar{v}_r^2 \frac{\Psi}{t_{Fr}}[C_L \cos\beta - C_D \sin\beta] \tag{1}$$

$$\frac{\partial Q}{\partial V} = \frac{1}{2}\rho_a \bar{v}_r^2 r \frac{\Psi}{t_{Fr}}[C_L \sin\beta + C_D \cos\beta] \tag{2}$$

with

$$\Psi = \frac{n_{Fb} C_{Fb}}{2\pi r},$$

Ψ is the solidity of the rotor and β is the angle between the relative velocity vector and the plane of rotation of the blade element.

In the numerical model, the pressure drop through the ACHE is modelled as a force exerted on the air in a direction opposite to the air flow direction. From design data for the modelled ACHE the pressure drop for normal flow conditions through the finned tube bundles is determined from the Robinson-and-Briggs correlation [9] for a six row tube bundle with round finned tubes in a staggered tube layout, i.e.

$$\mathrm{Eu} = \frac{\Delta p}{\rho_a v_{fr}^2}\left(\frac{A_c}{A_{fr}}\right)^2 = 120.016\left[\frac{m_a}{\mu_a A_{fr}}\right]^{-0.316}. \tag{3}$$

To determine a pressure drop coefficient, based on the frontal velocity of the ACHE, equation (3) can be rewritten in the following form:

$$K_{he} = 2\mathrm{Eu}\left(\frac{A_{fr}}{A_c}\right)^2 = 928.873\left[\frac{\rho_a v_{fr}}{\mu_a}\right]^{-0.316}. \tag{4}$$

Incoming flow streamlines approach the finned tube bundles at an angle and are then directed by the closely spaced fins to leave the finned tube bundles normally. The entering flow tends to separate at the leading edge of the tube fins, which results in an additional pressure loss. Moore and Torrence [10] quantified this pressure loss as follows:

$$K_{i\theta} = \left[\frac{1}{\sin\theta} - 1\right]^2, \tag{5}$$

with θ the angle between the approach velocity and the tube bundle. The value of $K_{i\theta}$ is restricted to $K_{i\theta} \leq 100$ [11].

The total pressure drop is a summation of the above-mentioned two pressure drop coefficients and is modelled as a force per unit volume exerted on the air in a direction opposite to the air flow direction:

$$\frac{\Delta p}{t_{tb}} = \left(\frac{-928.873(\rho_a v_{fr})^{0.684}\mu_a{}^{0.316}}{2t_{tb}} - \frac{\rho_a v_{fr}}{2tb}\left[\frac{1}{\sin\theta} - 1\right]^2\right)|v_{vr}|. \tag{6}$$

The entire ACHE fan unit is modelled and the heat transfer to the air by the ACHE is also taken into account. This ensures that the buoyancy forces, as well as the recirculation of warm plume air that can influence the air density at the fan inlet, are incorporated into the model.

The heat transfer is found by calculating the outlet air temperature, T_{ao}, as a function of the inlet air temperature, T_{ai}, the heat exchanger mean temperature, T_{he}, and the air mass flow rate,

m_a. If it is assumed that the mean heat exchanger temperature is constant the following equation can be derived from the heat exchanger effectiveness relation [12] for cross-flow conditions.

$$T_{ao} = T_{he} - (T_{he} - T_{ai}) \exp\left(-\frac{UA}{c_p m_a}\right). \tag{7}$$

The performance characteristics of the heat exchanger bundles are incorporated into the model by expressing the overall heat transfer coefficient as a function of the air mass flow rate. The air-side heat transfer coefficient in terms of the frontal velocity of the ACHE is determined with the aid of the Briggs-and-Young correlation [13], while the process fluid-side heat transfer coefficient, h_f, is assumed to be constant. With c_p also kept constant equation (7) can be rewritten as follows:

$$T_{ao} = T_{he} - (T_{he} - T_{ai}) \exp\left[-\frac{\left(\frac{1}{108392.6053 v_{fr}^{0.681}} + \frac{1}{223.19 h_f}\right)^{-1}}{36.06 c_p \rho_a v_{fr}}\right]. \tag{8}$$

The atmosphere is considered to be an infinitely large volume of air of homogeneous composition in a uniform gravitational field. The air is assumed to be incompressible and the local density is calculated from the ideal gas law:

$$\rho = \frac{p}{RT}, \tag{9}$$

where R is the gas constant.

All calculations were done for $T_{he} = 371.15$ K, $c_p = 1007.2$ J/kg K and $h_f = 1208$ W/m^{2}K.

Governing equations

PHOENICS provides solutions to the discretized version of sets of differential equations having the general form:

$$\text{div}(\rho \bar{v} \phi - \Gamma_\phi \nabla \phi) = S_\phi, \tag{10}$$

where ρ = density, $\bar{v}$ = velocity vector, $\phi = 1$, v_x, v_y, v_z, T, k and ε, Γ_ϕ = diffusion coefficient, S_ϕ = source term.

The expressions for S_ϕ and Γ_ϕ are specific to a particular meaning of ϕ and are given in Table 1.

The forces exerted by the fan blades on the air, as well as the pressure drop through the tube bundles, are incorporated in the force terms F_x, F_y and F_z.

Table 1. The forms of the diffusion coefficient and the source term in equation (10)

ϕ	S_ϕ	Γ_ϕ
1	0	0
V_x	$-\frac{\partial p}{\partial x} + \frac{\partial}{\partial x}\left(\mu_e \frac{\partial v_x}{\partial x}\right) + \frac{\partial}{\partial y}\left(\mu_e \frac{\partial v_y}{\partial x}\right) + \frac{\partial}{\partial z}\left(\mu_e \frac{\partial v_z}{\partial x}\right) + F_x$	μ_e
V_y	$-\frac{\partial p}{\partial y} + \frac{\partial}{\partial x}\left(\mu_e \frac{\partial v_x}{\partial y}\right) + \frac{\partial}{\partial y}\left(\mu_e \frac{\partial v_y}{\partial y}\right) + \frac{\partial}{\partial z}\left(\mu_e \frac{\partial v_z}{\partial y}\right) + F_y$	μ_e
V_z	$-\frac{\partial p}{\partial z} + \frac{\partial}{\partial x}\left(\mu_e \frac{\partial v_x}{\partial z}\right) + \frac{\partial}{\partial y}\left(\mu_e \frac{\partial v_y}{\partial z}\right) + \frac{\partial}{\partial z}\left(\mu_e \frac{\partial v_z}{\partial z}\right) + F_z + F_B$	μ_e
T	$\frac{1}{c_p}\left(v_x \frac{\partial p}{\partial x} + v_y \frac{\partial p}{\partial y} + v_z \frac{\partial p}{\partial z} + G\right)$	$\frac{\mu_e}{P_r}$
k	$G - \rho\varepsilon$	$\frac{\mu_e}{\sigma_k}$
ε	$\frac{\varepsilon}{k}(C_1 G - C_2 \rho \varepsilon)$	$\frac{\mu_e}{\sigma_\varepsilon}$

where $G = \mu_e\left\{2\left[\left(\frac{\partial v_x}{\partial x}\right)^2 + \left(\frac{\partial v_y}{\partial y}\right)^2 + \left(\frac{\partial v_z}{\partial y}\right)^2\right] + \left(\frac{\partial v_y}{\partial x} + \frac{\partial v_x}{\partial y}\right)^2 + \left(\frac{\partial v_y}{\partial z} + \frac{\partial v_z}{\partial y}\right)^2 + \left(\frac{\partial v_x}{\partial z} + \frac{\partial v_z}{\partial x}\right)^2\right\}$

The effect of the buoyancy force on the air is modelled via the Boussinesq variable density model and is incorporated in the body force term, F_B.

$$F_B = g(\rho - \rho_{ref}). \tag{11}$$

With the reference density, ρ_{ref}, equated to the ambient density, ρ_{aa}, this term gives the buoyancy force that arises from the differential variation of the density field about this mean. This has the effect of implicitly removing the hydrostatic variation of pressure from the pressure field. The absence of the hydrostatic component in the pressure field also simplifies the specification of the pressure boundary conditions, for often the so-called 'reduced pressure' is constant at the boundaries [14].

It is assumed that the k–ε model of Launder and Spalding [15] satisfactorily describes the turbulent nature of the flow.

The effective viscosity, μ_e, is given by

$$\mu_e = \mu + \mu_t, \tag{12}$$

where μ is the laminar dynamic viscosity of air and μ_t the turbulent eddy viscosity. The turbulent eddy viscosity is expressed as follows:

$$\mu_t = C_\mu \rho \frac{k^2}{\varepsilon}. \tag{13}$$

The Prandtl number in the temperature equation is taken as $Pr = 0.71$ and the empirical constants which appear in the turbulence equations are assigned the values shown in Table 2 [16].

The governing equations are discretized using the finite volume method as described by Patankar [17]. PHOENICS employs a staggered grid formulation and also uses the SIMPLEST pressure correction algorithm as described by Spalding [18]. A full description of PHOENICS is given by Rosten and Spalding [19–21].

Under-relaxation, using the false-time-step mode on the momentum, temperature, k and ε equations, and linear under-relaxation on the pressure and the other algebraic calculated values of density and turbulent eddy viscosity, are employed to ensure convergence.

Geometry and grid

One half of a bay of a long mechanical draught ACHE bank is considered. The computational domain is constructed in such a way that the physical dimensions of height, H_{he}, and the length of the fan inlet shroud, H_s, could easily be changed. The other geometrical dimensions of the ACHE are kept constant.

A body-fitted non-orthogonal coordinate system is used, consisting of $24 \times 69 \times 93$ cells in the x-, y- and z-directions, respectively. The grid is non-uniformly spaced so as to have a greater concentration of cells near the ACHE and the buoyant plume where more detailed information is required. The fan and the fan inlet shroud are modelled in a grid area of $20 \times 20 \times 10$ cells which are adapted to form a cylindrical pipe. A section of the computational grid around the fan is shown in Fig. 3.

The free atmospheric boundaries are placed far away from the ACHE, so as not to influence the flow field around the ACHE.

Boundary conditions

A dual-temperature boundary condition is applied at all the atmospheric boundaries. A zero gradient is prescribed at any point where outflow over the boundary occurs. When inflow over the

Table 2. Values of the constants in the turbulence equations

C_μ	C_1	C_2	σ_k	σ_ε
0.09	1.44	1.92	1.0	1.3

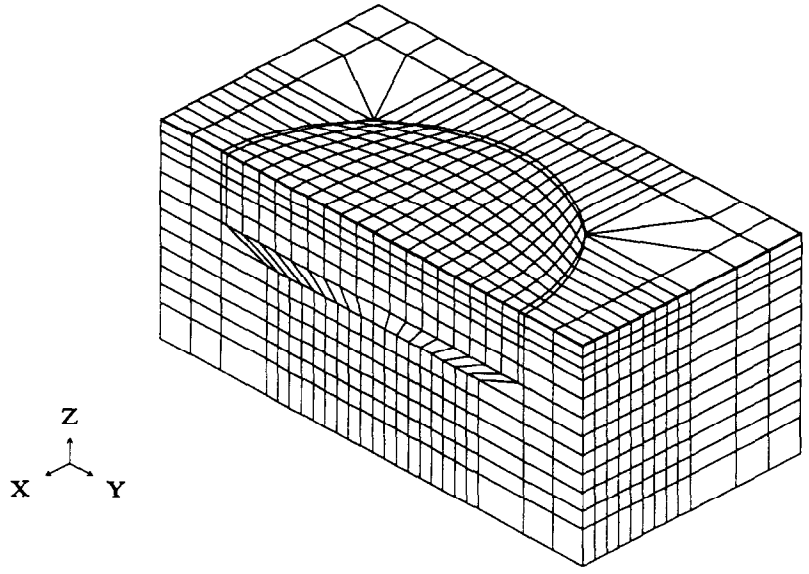

Fig. 3. A section of the computational grid around the fan.

boundary is encountered the temperature is assumed to be equal to the ambient temperature. A zero-gradient boundary condition is also prescribed for the variables, v_x, v_y, v_z, k and ε, while a zero value is assigned to the pressure, p, at the atmospheric boundary.

The first and last x-plane, as well as the y-plane where the ACHE bay is divided in two, are considered as symmetry planes. A zero-gradient boundary condition is prescribed for all the variables at these symmetry planes.

Wall functions as described by Launder and Spalding [16] are used to calculate values of variables near solid surfaces.

RESULTS

The volume flow rate of the ACHE fan, open on one side, is numerically determined for different heights of the ACHE platform. The length of cylindrical fan inlet shroud is kept constant ($H_s/d_F = 0.104$). To non-dimensionalize the results an ideal volume flow rate for the fan is determined by considering the same fan unit open on all four sides with the ratio of the ACHE (platform height)/(fan diameter) = 2.78. This is similar to the manner in which Salta and Kröger [7] determined the ideal volume flow rate in their experiments. According to them the actual air volume flow rate can be expressed in terms of this ideal flow rate and the heat exchanger geometry, i.e

$$V/V_{id} = 0.985 - e^{(-X)}, \tag{14}$$

with

$$X = \left(1 + \frac{45}{n_{F/b}}\right) H_{he}/(6.35 d_F).$$

Russell and Peachey [5, 6] also presented a non-dimensional curve as an indication of the influence of ACHE platform height on the fan performance of a forced-draught ACHE. The ideal volume flow rate in this instance was determined with the fan open on three sides with the ratio of the ACHE (platform height)/(fan diameter) = 2. They showed that there is good agreement between the trends of their experimental results and two data points from Spiers [4] and a single data point from Hart [6]. The current numerical results, as well as both the results from Salta and Kröger [7] and Russell and Peachey [5, 6], are plotted in Fig. 4. However, it is important to remember that only the trend of the Russell and Peachy curve can be compared to the other results and not the actual values, since the method of determining the ideal volume flow rate is not the same.

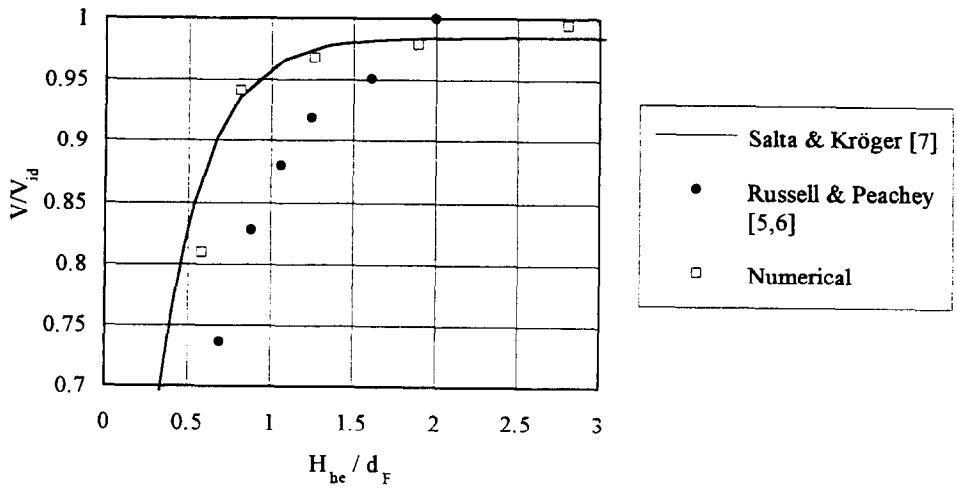

Fig. 4. The effect of the ACHE platform height on the fan performance.

A further aspect of the difference between the sets of results is that three different inlet shrouds are used in the experiments. In the numerical solutions, a cylindrical inlet shroud is used. Salta and Kröger [7] used a bell-mouth inlet shroud, while Russell and Peachey [5, 6], Spiers [4] and Hart [6] used a conical inlet shroud. In spite of these differences, the same trend can be observed. It is also shown in Fig. 4 that the numerical results for the cylindrical inlet and the correlation given by equation (14) compare very well.

To verify these results an experimental investigation is conducted. The experiments are done on the same apparatus as was used by Salta and Kröger [7], but differ in that cylindrical and conical fan inlet shrouds are used and that only an ACHE bay consisting of two axial fans is considered. The dimension ratio ($H_s/d_F = 0.104$) of the cylindrical inlet shroud corresponds to the ratio of the numerical model. The conical inlet shroud ratio corresponds to the experimental set-up of Russell and Peachey [5]. The dimensions of all the inlet shrouds are given in Fig. 5.

From the experimental results in Fig. 6, minor differences in the trends of the different fan inlet shrouds can be observed. Russell and Peachey [5] also did experiments with a cylindrical fan

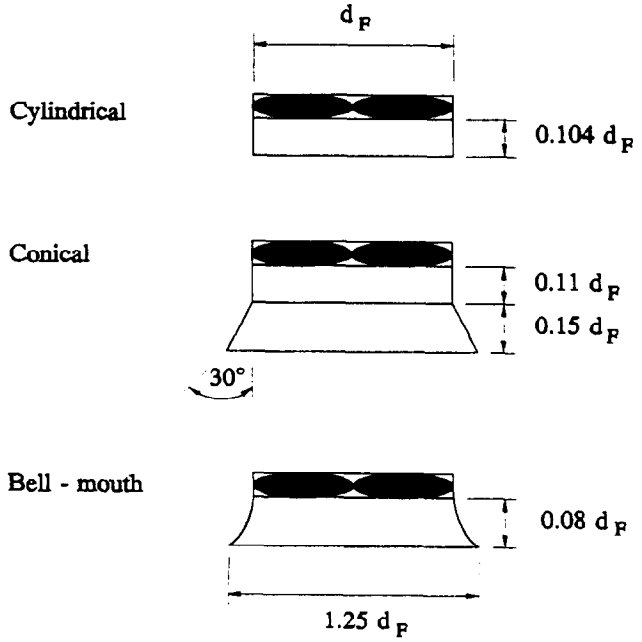

Fig. 5. The dimensions of the three fan inlet shrouds.

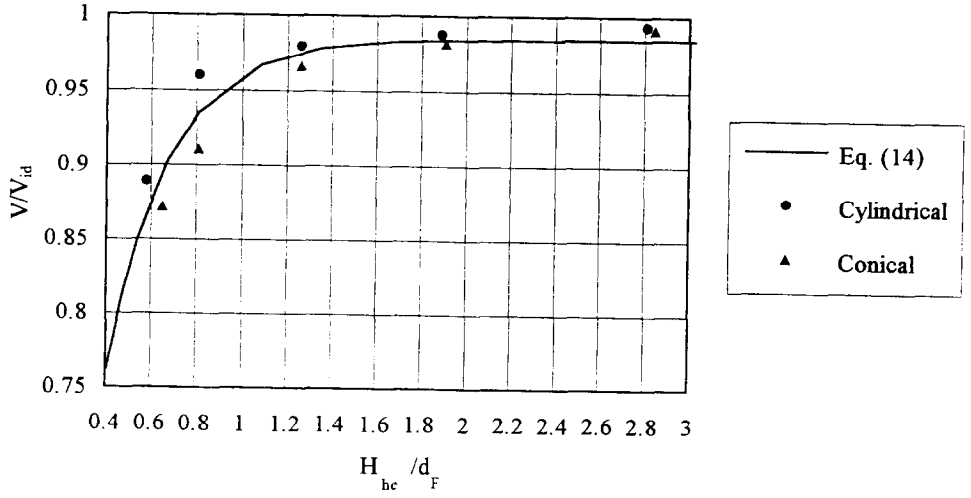

Fig. 6. The effect of ACHE platform height on the fan performance.

inlet shroud. Two different ACHE platform heights were considered. From the results it could be seen that the reduction in fan performance due to a lowering of the ACHE platform was not as severe for a cylindrical shroud as in the case of a conical shroud. This tendency can also be seen in Fig. 6. The fan performance with a bell-mouth shroud also tends to be less dependant on the ACHE platform height than the performance of the fans with a conical shroud and more dependant than the cylindrical shroud.

It can therefore be concluded from Fig. 6 that the trends for the three different fan inlet shrouds are very similar and it is recommended that when designing or evaluating an existing ACHE bank the correlation of Salta and Kröger [7] [equation (14)] be used to determine the influence of the ACHE platform height on the fan performance.

It is important to note that no comparison between the total volume flow rates delivered by the fans with different fan inlet shrouds can be drawn from Fig. 6, since the ideal volume flow rate for each fan system is specific to the type of fan inlet shroud used during the experimentation. The volume flow rates for the three different fan systems are shown in Fig. 7 as a percentage of the volume flow rate of the fan with the bell-mouth inlet shroud. Like Russell and Peachey [5] it is found that a fan performs better with a conical inlet shroud than with a cylindrical inlet shroud. In practice most fan suppliers recommend the more costly bell-mouth inlet shroud, since it experiences the lowest loss of the three [22].

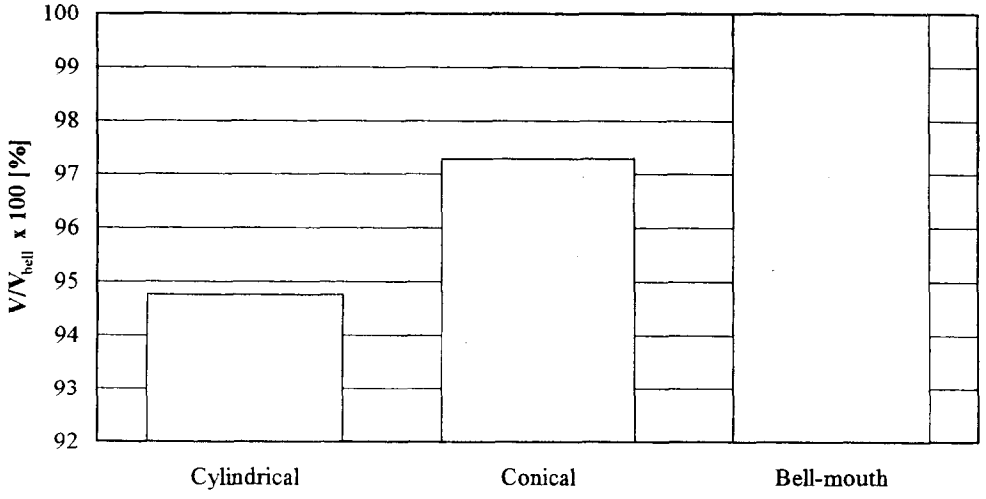

Fig. 7. A comparison between the volume flow rates for the three different fan systems.

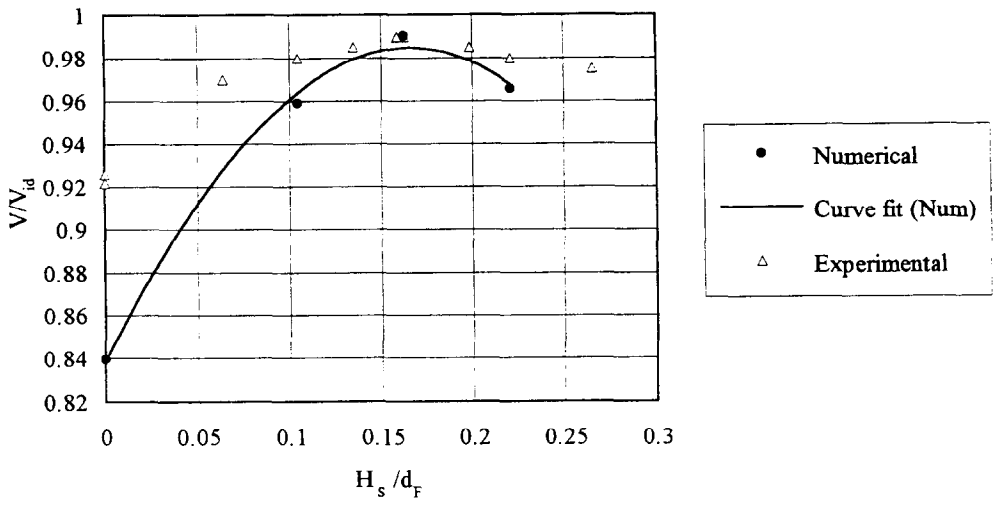

Fig. 8. The effect of the length of the cylindrical inlet shroud on the fan performance.

The effect of different lengths of a cylindrical fan inlet shroud is also numerically and experimentally investigated. The shroud length is changed while the ground clearance underneath the shroud inlet is kept constant $[(H_{he} - H_s)/d_F = 1.16]$. The results are non-dimensionalized by determining an ideal volume flow rate for the fan using the same fan unit with a cylindrical fan inlet shroud $(H_s/d_F = 0.104)$ open on all four sides. The ratio of the ACHE (platform height)/(fan diameter) = 2.78. The results are plotted in Fig. 8.

The difference between the numerical and experimental results can be attributed to the different fans (type and size) considered during the experiments and the numerical analysis, respectively. The fact that the same critical shroud length is reached at $H_s/d_F = 0.16$ emphasizes the wide applicability of this result. The inlet shroud shields the fan from the flow separation that occurs at the sharp corner of the ACHE platform. Flow separation also occurs at the inlet to the fan shroud, as can be seen from the pressure contour plot in Fig. 9. This separation area will also influence the fan performance. By lengthening the cylindrical shroud, this region is moved further away from the fan and the flow profile in the shroud begins to stabilize before reaching the fan. A critical length is however reached. Russell and Peachey [5] also found a reduction in fan performance experimentally by drastically lengthening the cylindrical fan inlet shroud.

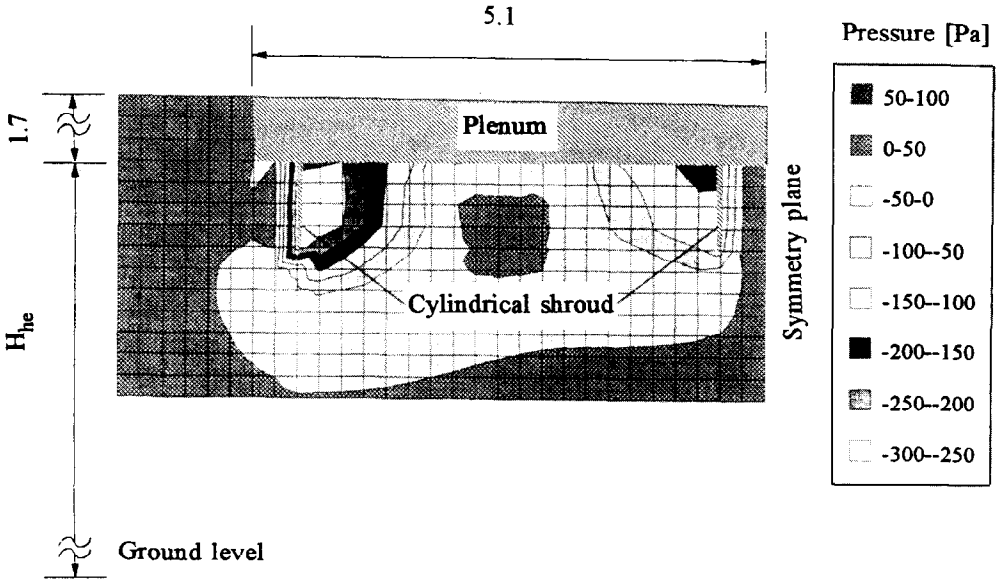

Fig. 9. A pressure contour plot at the inlet to the cylindrical fan inlet shroud.

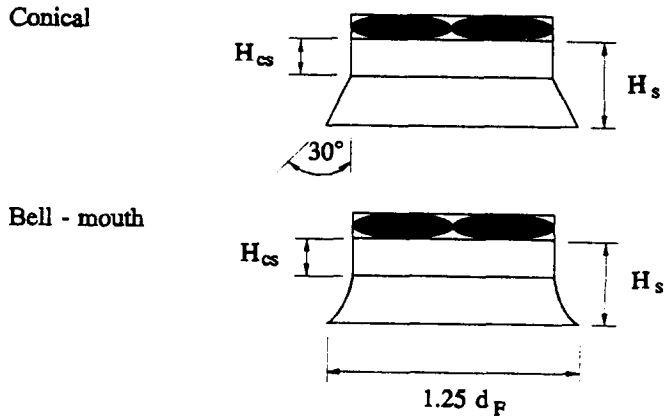

Fig. 10. Diagram of a conical inlet shroud and a bell-mouth inlet shroud.

A further experimental investigation is conducted to determine the optimal length of the cylindrical section (H_{cs}) of both the conical and bell-mouth inlet shrouds. A schematic illustration of the inlet shrouds is shown in Fig. 10. The same experimental procedure as in the case of the cylindrical inlet shroud is used. The results are non-dimensionalized by expressing the volume flow rates in terms of the highest volume flow rate determined for each of the two inlet shrouds, respectively.

From Fig. 11 it can be seen that the highest volume flow rates for both types of inlet shrouds are reached with no cylindrical section downstream of the cone or bell-mouth ($H_{cs} = 0.0$). Although these results are a first step in optimizing conical and bell-mouth inlet shrouds, other dimensions, like the cone angle and cone length for conical inlet shrouds and the elliptical shape of the bell-mouth inlet shrouds, will also have an influence on the fan performance.

CONCLUSIONS

In this study the effect of the ACHE platform height on the performance of a fan (part of a long ACHE bank) with different fan inlet shrouds is numerically and experimentally investigated. The results are compared with experimental data. It is concluded that the applicability of the correlation of Salta and Kröger [7] to determine the effect of the ACHE platform height on the fan performance can be extended to include all three fan inlet shrouds investigated. The results also illustrate the potential ability of the numerical approach to analyze an ACHE system.

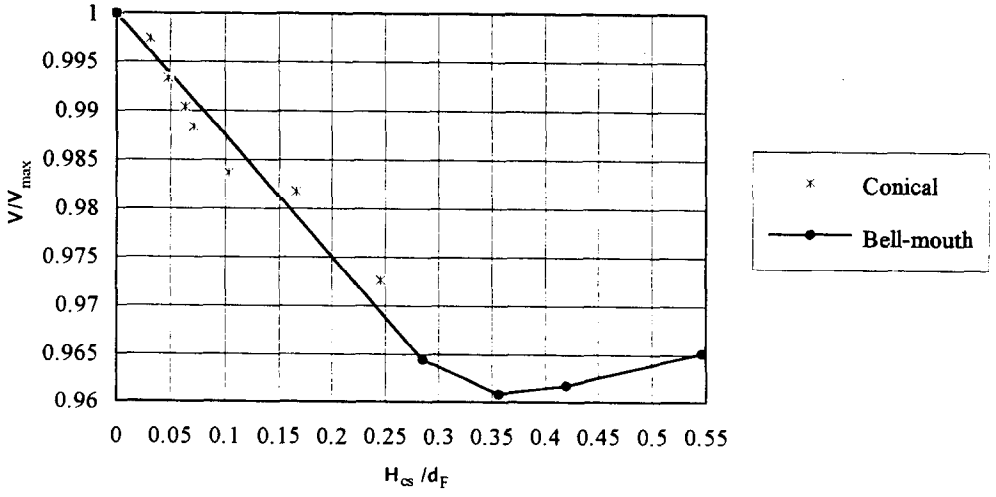

Fig. 11. The effect of a cylindrical section as part of a conical and bell-mouth inlet shroud on fan performance.

The investigation also shows that a critical length for a cylindrical shroud can be obtained and that conical and bell-mouth inlet shrouds should have no cylindrical sections upstream of the fan for optimal fan performance. These results emphasize the fact that the fan inlet shroud is an important feature of an ACHE and should be considered carefully when designing or evaluating the ACHE. Further investigations are currently under way to determine the optimal dimensions for conical and bell-mouth inlet shrouds.

REFERENCES

1. D. G. Kröger, Fan performance in air-cooled steam condensers. *Heat Recovery Systems & CHP* **14**(4), 391–399 (1994).
2. J. T. Turner, The aerodynamics of forced-draught air-cooled heat exchangers. *International Symp. on Cooling Systems*, BHRA Fluid Engineering, Cranfield, UK, pp. 81–99 (1975).
3. R. C. Monroe, Improving cooling tower fan system efficiencies. *Combustion Magazine* **50**(11) (1979).
4. R. R. M. Spiers, Inlet tests on a full size air-cooled heat exchanger. National Engineering Laboratories, NEL/HTFS 12, H.T.F.S. Paper RS 361, pp. 86–104 (1981).
5. C. M. B. Russell and J. Peachey, Air inflow effects on fan performance in air-cooled heat exchangers. *Conf. on Fan Design and Applications*, UK (1982).
6. C. M. B. Russell and R. J. Berryman, *The Calculation of Pressure Losses in Air-cooled Heat Exchanger Air Inlets and Plenum Chambers*. American Society of Mechanical Engineers, Heat Transfer Division, HTD Vol. 96. ASME, New York, USA, pp. 429–434 (1978).
7. C. A. Salta and D. G. Kröger, Effect of inlet flow distortion on fan performance in forced-draught air-cooled heat exchangers. *Heat Recovery Systems & CHP* **15**(6), 555–561 (1995).
8. G. D. Thiart and T. W. Von Backström, Numerical simulation of the flow field near an axial flow fan operating under distorted inflow conditions. *J. Wind Engng and Industrial Aerodynamics* (1992).
9. K. K. Robinson and D. E. Briggs, Pressure drop of air flowing across triangular pitch banks of finned tubes. *Chem. Engng Symp. Ser.* **64**(62), 177–184 (1966).
10. F. K. Moore and K. E. Torrence, Air flow in dry natural-draught cooling towers subject to wind. *Cornell Energy Report*. Cornell University, Ithaca, New York (1977).
11. C. G. Du Toit and J. C. B. Kotze, Air flow through a louvre and radiator core system. *Proc. Second National Symp. on Computational Fluid Dynamics*, Vereeniging, R.S.A., pp. 24–27, 52–61 (1991).
12. J. P. Holman, *Heat Transfer*, S.I. Metric Edition. McGraw-Hill, Singapore (1989).
13. D. E. Briggs and E. H. Young, Convective heat transfer and pressure drop of air flowing across triangular pitch banks of finned tubes. *Chem. Engng Symp. Ser.* **41**, 1–10 (1963).
14. D. Radosavljevic and D. B. Spalding, Simultaneous prediction of internal and external aerodynamic and thermal flow fields of a natural-draft cooling tower in a cross-wind. *Proc. Int. Cooling Tower Conf.*, EPRI GS-6317 (1989).
15. B. E. Launder, A. Morse, W. Rodi and D. B. Spalding, The prediction of free shear flows—a comparison of the performance of six turbulence models. *Proc. NASA Conf. on Free Shear Flows*, Langley (1972).
16. B. E. Launder and D. B. Spalding, The numerical computation of turbulent flows. *Comp. Meth. Appl. Mech. Engng* **3**, 269–289 (1974).
17. S. V. Patankar, *Numerical Heat Transfer and Fluid Flow*. McGraw-Hill, New York, p. 88 (1980).
18. D. B. Spalding, Mathematical Modelling of Fluid-mechanics, Heat Transfer and Chemical Reaction Processes: a Lecture Course, HTS/80/1, Imperial College, London (1980).
19. H. I. Rosten and D. B. Spalding, *The PHOENICS Equations*. TR/99, CHAM, Wimbledon, UK (1987).
20. H. I. Rosten and D. B. Spalding, *The PHOENICS Beginner's Guide*. TR/100, CHAM, Wimbledon, UK (1987).
21. H. I. Rosten and D. B. Spalding, *The PHOENICS Reference Manual*. TR/200, CHAM, Wimbledon, UK (1987).
22. Ventilatoren Stork Hengelo, General instructions for E-type fans, V.960874 (1985).